Weierstraß-Institut

für Angewandte Analysis und Stochastik

Leibniz-Institut im Forschungsverbund Berlin e. V.

Spectral properties of chimera states

Matthias Wolfrum[1], Oleh Omel'chenko[1,3], Serhiy Yanchuk[2], Yuri Maistrenko[3]

[1] Weierstraß-Institut für
    Angewandte Analysis und Stochastik
    Mohrenstraße 39
    10117 Berlin, Germany
    E-Mail: wolfrum@wias-berlin.de,
           omelchen@wias-berlin.de

[2] Institut für Mathematik,
    Humboldt-Universität zu Berlin
    Unter den Linden 6,
    10099 Berlin, Germany
    E-Mail: yanchuk@math.hu-berlin.de

[3] Institute of Mathematics,
    National Academy of Sciences of Ukraine,
    Tereshchenkivska Str. 3,
    01601 Kyiv, Ukraine
    E-Mail: y.maistrenko@biomed.kiev.ua

No. 1577

Berlin 2010

Abstract

Chimera states are particular trajectories in systems of phase oscillators with non-local coupling that display a spatio-temporal pattern of coherent and incoherent motion. We present here a detailed analysis of the spectral properties for such trajectories. First, we study numerically their Lyapunov spectrum and its behavior for an increasing number of oscillators. The spectra demonstrate the hyperchaotic nature of the chimera states and show a correspondence of the Lyapunov dimension with the number of incoherent oscillators. Then, we pass to the thermodynamic limit equation and present an analytic approach to the spectrum of a corresponding linearized evolution operator. We show that in this setting, the chimera state is neutrally stable and that the continuous spectrum coincides with the limit of the hyperchaotic Lyapunov spectrum obtained for the finite size systems.

Chimera states (see Figure 1) are remarkable spatio-temporal patterns where regions of synchrony coexist with regions of incoherent motion in a spatially homogeneous system of coupled oscillators. They constitute a new paradigm of dynamical behavior that can serve as a prototype for various physical phenomena, e.g. coexistence of synchronous and asynchronous neural activity (so called 'bump' states) [1, 2, 3, 4] or turbulent-laminar flow patterns [5]. For their mathematical description one has to employ concepts from the fields of pattern formation, deterministic chaos, and statistical physics. Indeed, starting with the pioneering work of Kuramoto [6], the thermodynamic limit of a large number of oscillators has been developed to a powerful tool for the investigation of chimera states. In this paper, we put our focus to the relation of chimera states in finite size systems to their thermodynamic limits. After a careful numerical study of the Lyapunov spectra for chimera trajectories in finite size systems, we compare our results with the spectral properties of the linearized evolution operator in the thermodynamic limit. We show that there the chimera states are neutrally stable and that their continuous spectrum coincides with the limit of the hyperchaotic Lyapunov spectrum obtained for the finite size systems.

1   Introduction

Systems of coupled phase oscillators have been widely used to study the basic properties of collective synchronization that can be observed in a huge variety of systems from physics, chemistry, biology, or social sciences [7, 8, 9, 10]. Recently, a new dynamical phenomenon occurring in such systems has attracted a lot of attention: Kuramoto e.a. [6, 11, 12] reported a new type of solutions that Strogatz e.a. [13, 14] later on called "chimera states" (see Figure 1), where a spatially homogeneous system of coupled identical oscillators displays self-organized

patterns of regions with synchronous and asynchronous motion. Since then such solutions have been observed under various conditions, including 1D and 2D arrays, inhomogeneous systems and systems with delayed coupling [15, 16, 17, 18, 19, 20, 21, 22, 23, 24, 25, 26, 27, 28, 29]. The main ingredients that are typically needed to observe chimera states are
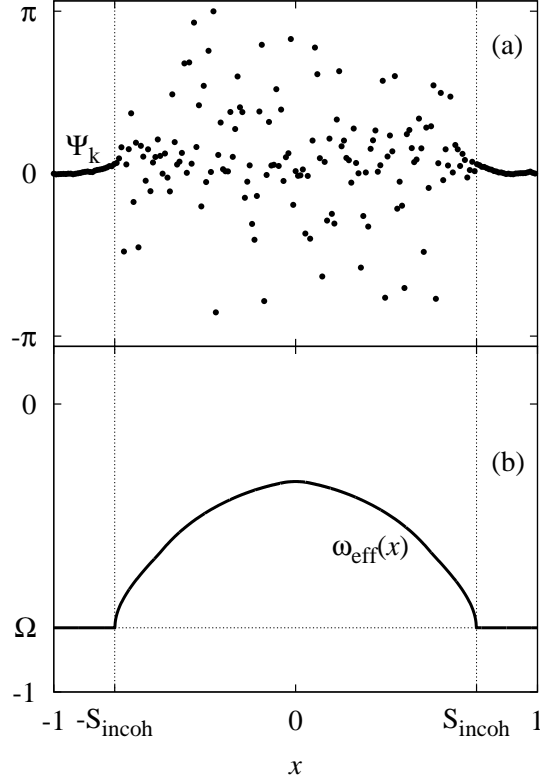

Figure 1: (a) Phase snapshot of a chimera state in system (1); (b) corresponding time averaged phase velocities $\omega_{\text{eff}}(x)$. Parameters: $N = 200$, $r = 0.7$, and $\alpha = 1.5$.

(i) a discrete medium, typically represented by a large number of oscillators distributed in space;

(ii) a non-local coupling that provides an interaction between local sub-populations with a coupling range that is different both from global and from local next neighbor coupling;

(iii) a well tuned amount of repulsion between the oscillators, that is typically achieved by a Sakaguchi phase lag parameter or a coupling delay.

Trying to reduce the numerical complexity, we choose for our studies a simple system comprising a ring of N identical non-locally coupled phase oscillators with phases $\Psi_1, \ldots, \Psi_N$ that

2

follow the evolution

$$\dot{\Psi}_k(t) = \omega - \frac{2}{N} \sum_{j=1}^{N} G(x_k - x_j) \sin(\Psi_k(t) - \Psi_j(t) + \alpha). \tag{1}$$

Here ω denotes the natural frequency of the oscillators that can be set to zero, and $\alpha \in (0, \pi/2)$ is a phase lag parameter. The oscillators are assumed to be uniformly distributed over the interval $[-1, 1]$ with positions $x_k = -1 + 2k/N$, $k = 1, \ldots, N$ and periodic boundary conditions. Using these positions we can employ a coupling function $G(x)$ to determine a non-local coupling on a macroscopic scale that is independent on the actual number of oscillators. In particular, throughout this paper we choose the simplest possible form of non-local coupling given by a step function

$$G_r(x) = \begin{cases} 1/(2r), & \text{if} \quad |x| \leq r, \\ 0, & \text{if} \quad |x| > r, \end{cases} \tag{2}$$

with $r \in (0, 1)$ denoting the radius of coupling.

Below, we put our focus to the spectral properties of chimera states both in finite size systems and in the thermodynamic limit. To this end, we employ the Lyapunov spectrum analysis, which is a standard tool for studying properties of chaotic systems [30, 31]. Recall that for N-dimensional system, there exists the set of N Lyapunov exponents, which are measures of how quickly small initial differences diverge or converge as two near-equivalent systems evolve. A positive exponent serves as a criterion for chaos, and hyperchaos is indicated by several positive exponents. Moreover, Lyapunov exponents give insight into many other dynamical features of chaotic trajectories: The full Lyapunov spectrum can be used to numerically determine the dimensionality [32] of a chaotic attractor. The inverse Lyapunov exponent is a characteristic time of mixing and of correlation delay. In the case of coupled systems, the synchronization threshold can be expressed in terms of the conditional Lyapunov exponents [33].

Lyapunov exponents for extended systems, e.g. lattices of coupled oscillators, have been studied in several papers. In particular, their statistics in disordered chaotic systems has been considered in [34], where an approximate expression for the distribution of their spacings is obtained. In [35] an example is shown, where the Lyapunov dimension approaches almost the total dimension of the phase space and the exponents tend to zero with systems size $N \to \infty$. A similar weak form of chaos was also reported in [36] with the scaling behavior of the Lyapunov exponents of a periodically oscillating collective state as N^{-2}. In the context of spatio-temporal chaos, the very existence of a well-defined Lyapunov spectrum in the thermodynamic limit is a proof of the extensivity of chaos [31, 37, 38].

The paper is organized as follows. In Section 2 we present our numerical results for the Lyapunov spectrum of chimera states. In particular, we study the dependence on the parameters α and r, calculate the Lyapunov dimension, and analyze the scaling behavior for an increasing number N of oscillators at different parts of the spectrum.

In the following section, we shortly recall the derivation of a thermodynamic limit system for $N \to \infty$. Then we use its linearization to study the spectral properties of the evolution operator in the corresponding infinite dimensional system. Similarly as in the results of Mirollo and Strogatz [39, 10] for locked or partially locked states in the classical Kuramoto system, we find

continuous spectrum on the imaginary axis that indicates a neutral stability of the corresponding states. We show that the real parts of this continuous spectrum coincides with the limit for $N \to \infty$ of the Lyapunov spectrum calculated before.

2 Lyapunov spectrum

In this section, we present our numerical results for the Lyapunov spectrum of chimera states and its dependence on various parameters. In particular, we discuss the scaling behavior for $N \to \infty$ of the Lyapunov exponents and of the Lyapunov dimension. Our numerical computations employed a commonly used fourth-order Runge-Kutta scheme (with fixed time step $dt = 0.01$) to integrate system (1) together with the standard algorithm for Lyapunov exponents using continuous Gram-Schmidt orthonormalization [40]. Simulations extend typically over 60000 time units that seems to provide a stabilization of the Lyapunov exponents at a satisfactory level of accuracy.

To compare the Lyapunov spectra for different numbers of oscillators N we represent the sequence λ_k of non-increasing Lyapunov exponents by the function $\Lambda_N(\nu)$, $0 \le \nu \le 1$ such that $\Lambda_N(\nu) = \lambda_k$ if $\nu = (k-1)/(N-1)$. Figure 2 shows the Lyapunov spectra for chimera states in system (1) with $N = 100$, $\alpha = 1.44$ and three different values of the coupling radius r. Each spectrum contains a considerable number of positive Lyapunov exponents indicating the

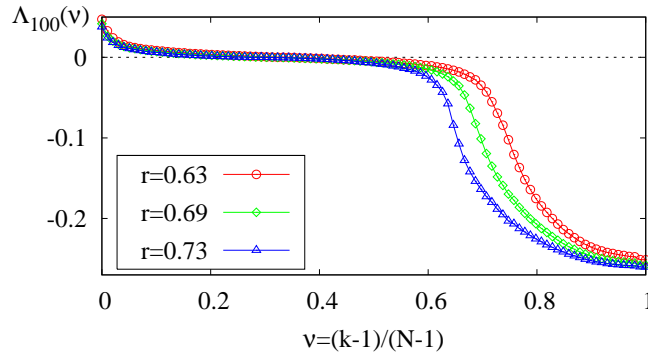Figure 2: (Color) Lyapunov spectra $\Lambda_{100}(\nu)$ computed for chimera trajectories of (1) with coupling radius $r = 0.63$ (red circles), 0.69 (green diamonds), and 0.73 (blue triangles), and phase lag $\alpha = 1.44$.

hyperchaotic nature of the chimera states. One exponent is exactly equal to zero and reflects the phase shift symmetry of the system (1). Also the index shift symmetry of the system (1), which is a discrete symmetry for finite N and tends to a continuous symmetry in the case $N \to \infty$, induces an exponent close to zero.

In Figure 3 we show the maximal Lyapunov exponent $\lambda_{\max} = \Lambda_{100}(0)$ for all values of parameters (r, α) where a chimera state was detected. The Figure shows clearly that the maximal Lyapunov exponent remains positive and separated from zero for all parameters (r, α) in this region.
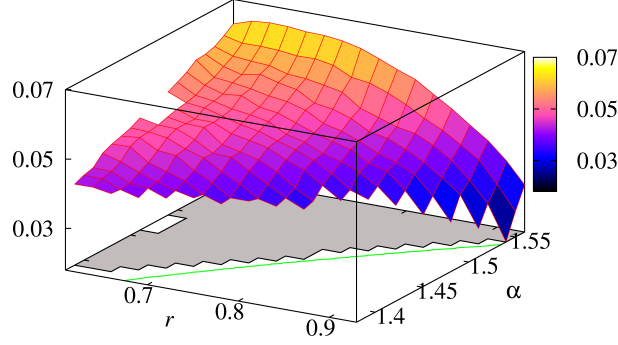
4

Figure 3: (Color) Dependence of the maximal Lyapunov exponent $\lambda_{\max} = \Lambda_{100}(0)$ on the coupling radius r and the phase lag α. The gray region at the bottom indicates the parameter region, where we found chimera trajectories for $N = 100$, the green line indicates the boundary of the existence region for chimera states in the thermodynamic limit $N = \infty$.

Varying the coupling radius r or, alternatively, the phase lag α, we obtain typically chimera states with different sizes of the coherent and incoherent regions. This size can be represented by the relative number of incoherent oscillators $S_{incoh} = N_{incoh}/N$ that is a macroscopic quantity and can be obtained from Kuramoto's self-consistency equation in the thermodynamic limit $N \to \infty$ (see [6]).

In Figure 2 we present the Lyapunov spectra for three different values of the coupling radius r that correspond to different sizes of the coherent region. One can observe that there is almost no difference for the positive Lyapunov exponents whereas the stable part of the spectrum is shifted, leading to an increasing number of strongly stable exponents for larger r and correspondingly larger size of the coherent region. Indeed, it is natural to assume that perturbations that are localized in the coherent region contribute to the stable part of the spectrum whereas perturbations localized in the incoherent region can contribute to the chaotic part of the spectrum.

This observation can be made more precise by comparing the corresponding Lyapunov dimensions (see Figure 4(a)). Recall that for a given Lyapunov spectrum $\{\lambda_k\}$ the Lyapunov dimension is given by

$$D_L = K + \sum_{j=1}^{K} \frac{\lambda_j}{|\lambda_{K+1}|},$$

where K is the maximum integer such that the sum of the K largest Lyapunov exponents is still non-negative. Our numerical results show that the relative Lyapunov dimension $d_L = D_L/N$ is slightly smaller, but follows the change of the size of the incoherent region S_{incoh}, see Figure 4(a). The observed gap $S_{incoh} - d_L$ that has still a size of 5% can be presumably a finite N effect that will vanish for larger numbers of N. However, our numerical results (see Figure 4(b)), due to the enormous computational complexity covering only the range up to $N = 120$, do not show this trend very clearly. Besides the Lyapunov dimension D_L, we also consider the point-wise scaling properties of the Lyapunov spectrum as the number of oscillators N increases (see Figure 5). As default parameters we use $r = 0.7$ and $\alpha = 1.5$. The maximum
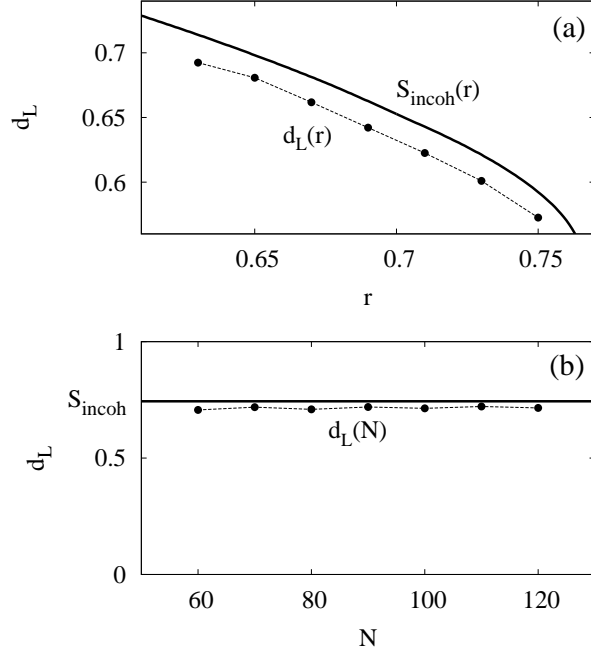
Figure 4: Relative Lyapunov dimension (dots) and relative size of the incoherent region S_{incoh} (solid line): (a) for varying coupling radius r, and $\alpha = 1.44$, (b) for varying system size N, and $r = 0.7, \alpha = 1.5$.

number for which we were able to calculate a full Lyapunov spectrum is $N = 120$. The leading part of the spectrum has been calculated for N up to 300. We compare these spectra with the real part of the spectrum, calculated analytically by means of a thermodynamic limit analysis (see following section). It turns out that for $0 \leq \nu \leq S_{incoh}$ the Lyapunov exponents converge to zero for $N \to \infty$, whereas for $S_{incoh} < \nu \leq 1$ they have a non-zero negative limit. Our numerical calculations (compare Figure 6), show that there are three different types of scaling behavior for different parts of the spectrum:

(i) The maximal Lyapunov exponent $\lambda_{\max} = \Lambda_N(0)$ scales as $N^{-1/2}$.

(ii) For all $\nu \in (0, S_{incoh})$ the Lyapunov exponents $\Lambda_N(\nu)$ scale roughly as N^{-1}

(iii) For $\nu \in (S_{incoh}, 1]$ the Lyapunov exponents $\Lambda_N(\nu)$ tend to some negative limit $\Lambda_\infty(\nu)$.

The different types of scaling behavior apparently reflect the different nature of the corresponding Lyapunov exponents. In particular, the scaling law $\sim N^{-1}$ has been similarly observed in the globally coupled Kuramoto system [35]. In contrary, the scaling law of the maximal Lyapunov exponent indicates existence of a stronger macroscopic mode that is peculiar to the chimera state and has not been observed in a globally coupled system.
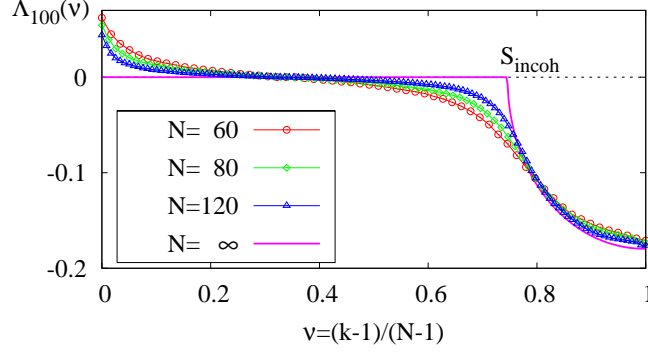
6

Figure 5: (Color) Lyapunov spectra $\Lambda_{100}(\nu)$ computed for chimera trajectories of (1) with system size $N = 60$ (red circles), 90 (green diamonds), and 120 (blue triangles). Other parameters: $r = 0.7, \alpha = 1.5$.

3   Thermodynamic limit analysis

In this section we present an analytic approach to the stability properties and the spectrum of a chimera state using the thermodynamic limit $N \to \infty$. First, we will recall briefly the derivation of a dynamical equation for this limit, following the approach of Pikovsky and Rosenblum [41]. The chimera states appear in this system as a stationary state in a properly chosen co-rotating frame. Finally we will use the linearization at such a state in order to study its spectral properties.

3.1   The dynamical equation for $N = \infty$

System (1) can be rewritten in the equivalent form

$$\dot{\Psi}_k(t) = \omega + \text{Im} \left(Z_k(t) e^{-i\Psi_k(t)} \right), \tag{3}$$

where

$$Z_k(t) = \frac{2}{N} \sum_{j=1}^{N} G(x_k - x_j) e^{i\Psi_j(t)} e^{-i\alpha} \tag{4}$$

is the effective force acting on the k-th oscillator. We consider now the oscillators in a small vicinity of any point x and describe them as a sub-population of globally coupled oscillators. This is asymptotically correct in a thermodynamic limit where together with $N \to \infty$ also the number of sub-populations tends to infinity. The collective behavior of the sub-populations is then characterized by a local complex mean field $z(x, t)$ defined according to

$$z(x, t) := \lim_{N \to \infty} \frac{1}{|B_\delta^N(x)|} \sum_{j \in B_\delta^N(x)} e^{i\Psi_j(t)}, \tag{5}$$

where $B_\delta^N(x) = \{j : 1 \leq j \leq N, |x - x_j| < \delta\}$ denotes a neighborhood of the point x. For the limit, we assume $\delta = \delta(N) \to 0$ for $N \to \infty$ in a way that the number of points $|B_\delta^N(x)|$
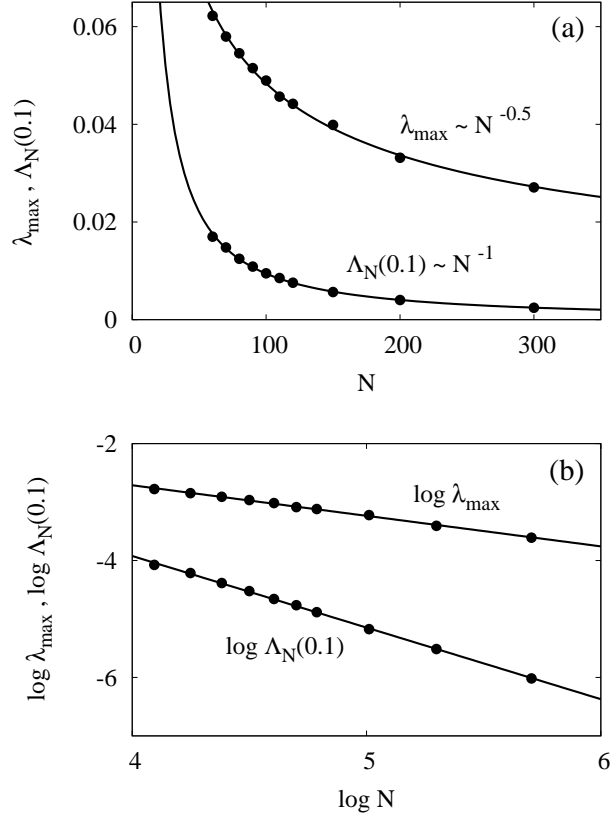
7

Figure 6: Scaling behavior of the maximal Lyapunov exponent $\lambda_{\max} = \Lambda_N(0)$ and of the intermediate Lyapunov exponent $\Lambda_N(0.1)$. (a) Natural and (b) logarithmic scale. Fitted lines $\lambda_{\max} \sim N^{-0.52}$ and $\Lambda_N(0.1) \sim N^{-1.2}$. Parameters: $r = 0.7$, $\alpha = 1.5$.

in the neighborhood at the same time tends to infinity. Note that (5) implies $0 \leq |z(x,t)| \leq 1$ for all x and t. For $|z(x,t)| = 1$ the oscillators around point x are synchronized in phase, while $|z(x,t)| = 0$ corresponds to the local absence of phase synchronization. For a chimera state, $|z(x,t)| = 1$ identifies the coherent domain, while $|z(x,t)| < 1$ holds true in the incoherent domain.

Interpreting now the space variable x as a sub-population index and following the approach of Pikovsky and Rosenblum [41], we obtain an integro-differential equation for the effective dynamics of the local mean field $z(x,t)$

$$\frac{\partial z}{\partial t} = i\omega z(x,t) + \frac{1}{2}Z(x,t) - \frac{z^2(x,t)}{2}Z^*(x,t), \tag{6}$$

where

$$Z(x,t) = e^{-i\alpha} \int_{-1}^{1} G(x-y)z(y,t)dy, \tag{7}$$

and the symbol $*$ denotes the complex conjugate.

8

The derivation of this system (for details see [41]) is based mainly on the application of the Watanabe-Strogatz theory [42, 43]. Alternatively, Eq. (6)-(7) can also be derived in a different way, using the Ott-Antonsen method [44, 45] and a probabilistic interpretation of the function $z(x,t)$. This approach, together with a variety of examples, including our system (1), has been referred recently in [20].

It is assumed that all macroscopic properties of the chimera states as well as the typical bifurcation scenarios involving them can be explained in terms of the solutions of Eq. (6)-(7). However, there is a lack of rigorous mathematical theory, telling in which sense the solutions to (6)-(7) can be interpreted as an approximation of solutions to the original equation (1) for large N.

Anyhow, Eq. (6)-(7) constitutes a significant simplification with respect to the original equation, since we expect that for any statistically stationary solution of system (1) which might be very different for neighboring indices k, the corresponding mean field solution $z(x,t)$ of Eq. (6)-(7) is a continuous function of both x and t.

3.2 Standing wave solutions

It is known [20] that a chimera state in the original Eq. (1) corresponds to a standing wave solutions of Eq. (6)-(7). Recalling the phase shift symmetry we transform system (6)-(7) into rotating coordinates

$$\hat{z}(x,t) = e^{-i\Omega t}z(x,t) \tag{8}$$

and obtain

$$\frac{\partial \hat{z}}{\partial t} = i\Delta\hat{z}(x,t) + \frac{1}{2}\hat{Z}(x,t) - \frac{\hat{z}^2(x,t)}{2}\hat{Z}^*(x,t), \tag{9}$$

where we used the abbreviation $\Delta := \omega - \Omega$ and the co-rotating non-local coupling force

$$\hat{Z}(x,t) = e^{-i\alpha}\int_{-1}^{1} G(x-y)\hat{z}(y,t)dy = Z(x,t)e^{-i\Omega t}. \tag{10}$$

We seek now for stationary solutions

$$\hat{z}(x,t) \equiv \hat{z}(x) \tag{11}$$

of the resulting system together with their rotation frequency Ω. The time-independent profiles $\hat{z}(x)$ and $\hat{Z}(x)$ satisfy the quadratic equation

$$\hat{Z}^*(x)\hat{z}^2(x) - 2i\Delta\hat{z}(x) - \hat{Z}(x) = 0, \tag{12}$$

that can be solved by

$$\hat{z}_{1,2}(x) = \frac{i\Delta \pm \sqrt{|\hat{Z}(x)|^2 - \Delta^2}}{\hat{Z}^*(x)}. \tag{13}$$

Taking into account (10), this is still an implicit equation for $\hat{z}(x)$. Note that in general there are two solution branches in formula (13) corresponding to the plus and minus signs at the

square root. As we will explain below, we can restrict here to the branches $+\sqrt{a}$ for positive a and $-i\sqrt{-a}$ for negative a.

Inserting (13) into (10) we obtain finally the self-consistency equation (cf. Eq. (5) in [13])

$$\hat{Z}(x) = e^{-i\alpha} \int_{-1}^{1} G(x-y) \frac{i\Delta + \sqrt{|\hat{Z}(y)|^2 - \Delta^2}}{\hat{Z}^*(y)} dy. \tag{14}$$

This nonlinear integral equation can be easily solved numerically via an appropriate discretization, see e.g. [6, 13]. In order to obtain a uniquely solvable problem, one has to fix the spatial position of the inhomogeneous profile $\hat{Z}(x)$. For this purpose, we require that the minimum of $|\hat{Z}(x)|$ is attained at point $x = 0$. This implies that the incoherent region of a corresponding chimera state is centered around zero. Under this additional assumption (14) has a solution pair $(\hat{Z}(x), \Delta)$ that is locally unique up to a complex phase shift of the function $\hat{Z}(x)$.
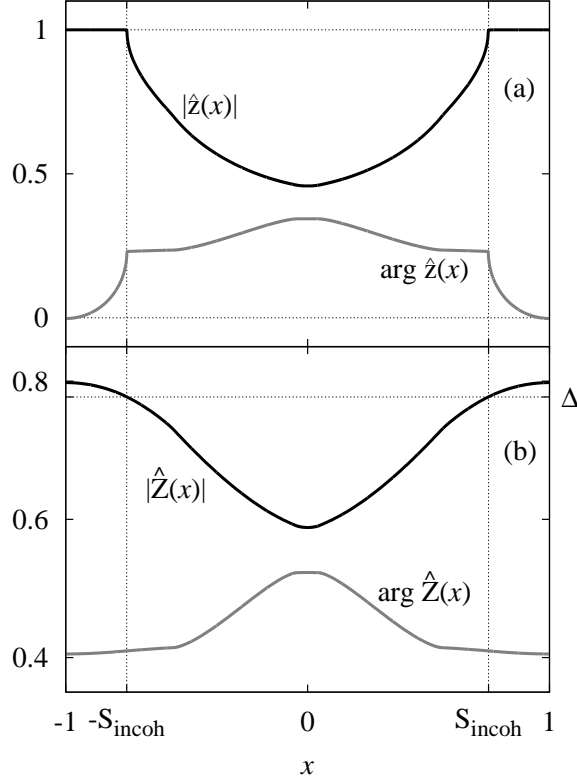

Figure 7: Solutions of self-consistency equation (13), (14). (a) Local mean field $\hat{z}(x)$, (b) corresponding non-local coupling force $\hat{Z}(x)$. Parameters: $r = 0.7$, $\alpha = 1.5$.

The boundaries $x = \pm S_{incoh}$ of the incoherent region, that we assumed to be centered around $x = 0$, are determined by the condition

$$S_{incoh} = \min\{x \in [0,1] : |\hat{z}(x)| = 1\}.$$

10

In terms of $\hat{Z}(x)$ the condition for the interface S_{incoh} is given by $|\hat{Z}(x)| = |\Delta|$. Indeed, for

$$|\hat{Z}(x)| \geq |\Delta|$$

the expression under the square root in Eq. (13) is positive and one can easily derive that $|\hat{z}_{1,2}(x)| = 1$ there. Hence this condition characterizes the coherent region.

For $|\hat{Z}(x)| < |\Delta|$, we obtain from (13) that

$$|\hat{z}_{1,2}(x)| = \frac{2\Delta \left(\Delta \pm \sqrt{\Delta^2 - |\hat{Z}(x)|^2} \right)}{|\hat{Z}(x)|}.$$

Concluding from (12) that $|\hat{z}_1||\hat{z}_2| = 1$, we see that as soon as $|\hat{z}_1| \neq |\hat{z}_2|$ only the branch $\hat{z}_2(x)$ that uses the negative sign satisfies $|\hat{z}_2(x)| < 1$ and allows for an interpretation as a local mean field of coupled oscillators. This justifies one part of our choice for the branches of the square root given above.

3.3 Lyapunov spectrum in the thermodynamic limit

We are now going to analyze the stability properties of a stationary profile $\hat{z}(x)$. To this end, we will linearize Eqs. (9)-(10) and study the spectrum of the resulting linear operator. A similar spectral problem for a continuum limit of a coupled oscillator system has already been considered in [10] and [39]. The results in [10] show that the stability of partially locked states in the classical Kuramoto system can be analyzed by means of the spectrum of the linearization in a suitable continuum limit. The main result in that paper was that the partially locked states have a neutrally stable continuous spectrum that can be attributed to the incoherent motion of the unlocked oscillators that are present in such solutions. Additionally, stable continuous spectrum on the real axis as well as stable point spectrum has been found for this state. A major achievement of Mirollo and Strogatz in [10] is also to clarify the mathematical background of their continuum limit in terms of probability measure spaces and functional analytic properties of linearization operators acting on such spaces.

In the sequel, we will follow a similar approach for the stability properties in the chimera problem. In particular, we will analytically calculate the neutral and stable continuous spectrum, in a similar way as in [10]. However, we will avoid mathematical details as much as possible and refer the reader to [10] for more mathematical background. Instead, we finally compare the analytically obtained spectrum with the numerically obtained Lyapunov spectra shown above.

For the variations $\hat{v}(x,t)$ around a given stationary profile $\hat{z}(x)$ we obtain after linearizing system (9)-(10) the linear equation

$$\frac{\partial \hat{v}}{\partial t} = \mu(x)\hat{v}(x,t) + \frac{1}{2}\hat{V}(x,t) - \frac{\hat{z}^2(x)}{2}\hat{V}^*(x,t), \tag{15}$$

where $\hat{V}(x,t)$ is the local mean field for $\hat{v}(x,t)$ as in (10) and

$$\mu(x) = i\Delta - \hat{z}(x)\hat{Z}^*(x) = -\sqrt{|\hat{Z}(x)|^2 - \Delta^2}. \tag{16}$$

11

Remark that the latter identity is a trivial consequence of (13). Note that (15) together with (16) and the definition of the local mean field $\hat{V}(x, t)$ according to (10) can be written as an operator equation

$$\frac{d\hat{v}}{dt} = (\mathbf{M} + \mathbf{K})\hat{v}(t). \tag{17}$$

where the multiplication operator $\mathbf{M}$ is defined as multiplication with $\mu(x)$ and $\mathbf{K}$ contains the remaining terms of (15) that depend linearly on $\hat{v}$ via the local mean field integral. In order to avoid complications caused by the complex conjugation, we reformulate this equation for complex $\hat{v}$ now as a system for two real components

$$\hat{\mathbf{v}}(t) = \begin{pmatrix} \text{Re } \hat{v}(x, t) \\ \text{Im } \hat{v}(x, t) \end{pmatrix},$$

where the vector-function $\hat{\mathbf{v}}(t)$ assumes values in the functional space

$$\mathcal{L}_{per}^2 := \{u \in L^2((-1, 1); \mathbb{R}^2) : u \text{ is 2-periodic}\}.$$

Then, the multiplication operator $\mathbf{M}$ is given by

$$\mathbf{M} = \begin{pmatrix} \text{Re } \mu(x) & -\text{Im } \mu(x) \\ \text{Im } \mu(x) & \text{Re } \mu(x) \end{pmatrix}$$

and $\mathbf{K}$ is the integral operator

$$(\mathbf{K}\hat{\mathbf{v}})(x) = \begin{pmatrix} \int_{-1}^{1} [K_{11}(x, y)\hat{v}_1(y) + K_{12}(x, y)\hat{v}_2(y)] \, dy \\ \int_{-1}^{1} [K_{21}(x, y)\hat{v}_1(y) + K_{22}(x, y)\hat{v}_2(y)] \, dy \end{pmatrix}$$

with the (2×2)-matrix kernel

$$K(x, y) = \left[Q - Q^T \begin{pmatrix} \text{Re } \hat{z}^2(x) & \text{Im } \hat{z}^2(x) \\ \text{Im } \hat{z}^2(x) & -\text{Re } \hat{z}^2(x) \end{pmatrix} \right] G(x - y),$$

where

$$Q = \begin{pmatrix} \cos \alpha & \sin \alpha \\ -\sin \alpha & \cos \alpha \end{pmatrix}$$

and Q^T denotes the transpose of matrix Q.

For any piecewise continuous coupling function $G(x)$, as e.g. our default choice $G(x) = G_r(x)$, a corresponding stationary profile $\hat{Z}(x)$ of the self-consistency equation (14) turns out to be continuous in x. Hence, both operators $\mathbf{M}$ and $\mathbf{K}$ are linear bounded operators from $\mathcal{L}_{per}^2$ to $\mathcal{L}_{per}^2$. The stability properties of the stationary solution to Eq. (6) can now be investigated by analyzing the spectrum of the corresponding linearization given by the operator $\mathbf{M} + \mathbf{K}$.

Following the general spectral theory for a linear operator A, we distinguish between different types of spectrum. The point spectrum $\sigma_p(A)$ contains all complex values λ where $\lambda I - A$

has a kernel and hence is not invertible. The continuous spectrum $\sigma_c(A)$ contains values λ for which $\lambda I - A$ has no kernel, but the inverse $(\lambda I - A)^{-1}$ is an unbounded operator that is defined only on a dense subspace.

Taking into account the uniform boundedness of the kernel matrix $K(x, y)$ we conclude that the integral operator $\mathbf{K}$ is a compact operator from $\mathcal{L}^2_{per}$ to $\mathcal{L}^2_{per}$. Therefore, according to Weyl's result (see e.g. [46]), the continuous spectrum $\sigma_c(\mathbf{M}+\mathbf{K})$ is given just by $\sigma_c(\mathbf{M})$. The continuous spectrum $\sigma_c(\mathbf{M})$ consists of all complex values λ with

$$\det \begin{pmatrix} \mathrm{Re}\ \mu(x) - \lambda & -\mathrm{Im}\ \mu(x) \\ \mathrm{Im}\ \mu(x) & \mathrm{Re}\ \mu(x) - \lambda \end{pmatrix} = 0 \tag{18}$$

for some $x \in [-1, 1]$. Indeed, one can easily check that in this case the image of the operator $\lambda I - \mathbf{M}$ is only a dense subspace of $\mathcal{L}^2_{per}$. Hence, we obtain from (16) that

$$\sigma_c(\mathbf{M}) = \left\{ \mu(x) \ \middle|\ 0 \leq x \leq 1 \right\} \cup \{c.c.\}$$

$$= \left\{ -\sqrt{|\hat{Z}(x)|^2 - \Delta^2} \ \middle|\ 0 \leq x \leq 1 \right\} \cup \{c.c.\} \tag{19}$$

For a chimera solution of (14) this spectrum consists of two parts (see Figure 8). The first part is the interval $[-|\mu(1)|, 0]$ on the real axis, and the second part is the interval $[-i|\mu(0)|, i|\mu(0)|]$ on the imaginary axis. At this point we can also provide the missing argument for our choice of the solution branches in (13): choosing the opposite sign there, the real branch of $\sigma_c(\mathbf{M})$ is located in the positive half plane and the corresponding chimera would be unstable.

We compare now the real parts of the continuous spectrum parametrized by $x \in [0, 1]$ according to formula (19), with the Lyapunov spectrum functions $\Lambda_N(x)$ of the corresponding chimera state (see Figure 5). Recalling our numerical results about the limit behavior for $N \rightarrow \infty$, we observe for $0 \leq x \leq S_{incoh}$ a convergence of the Lyapunov spectrum to the corresponding neutral part of the continuous spectrum. At the same time, we observe for $S_{incoh} < x \leq 1$ a good coincidence of the stable Lyapunov spectrum with the stable continuous spectrum. Hence we conclude that the spectrum in the thermodynamic limit

$$\Lambda_\infty(x) := \begin{cases} 0, & \text{if} \quad 0 \leq x \leq S_{incoh}, \\ -\sqrt{|\hat{Z}(x)|^2 - \Delta^2}, & \text{if} \quad S_{incoh} < x \leq 1, \end{cases} \tag{20}$$

can be considered as the limit of the spectra $\Lambda_N(x)$ for $N \rightarrow \infty$. Additional evidences for this claim can be obtained if we compare the Lyapunov spectra on Figure 2 with the corresponding Lyapunov spectrum functions $\Lambda_\infty(\nu)$ as it is shown on Figure 9.

It is clear that the composed operator $\mathbf{M} + \mathbf{K}$ should also have a point spectrum. However, for the chimera states we studied, there seems to be no point spectrum affecting strongly their stability properties. But we presume that at the boundary of existence of stable chimera states, critical point spectrum might be responsible for inducing an instability with respect to a collective mode.
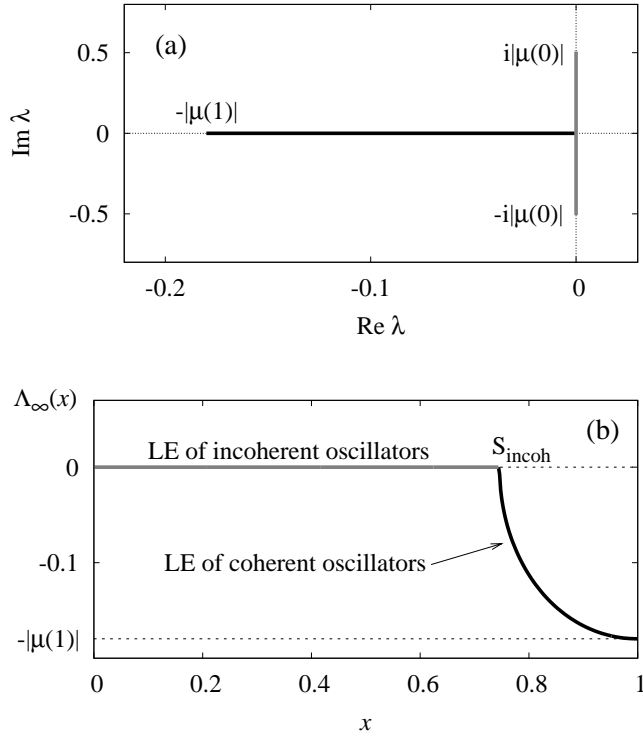
Figure 8: (a) Continuous spectrum $\sigma_c(\mathbf{M})$ of a chimera state in system (1) with $r = 0.7$ and $\alpha = 1.5$. (b) Corresponding Lyapunov spectrum function $\Lambda_\infty(x)$ according to (20).

4 Conclusions

Starting with the pioneering works of Kuramoto, the chimera states are known as a peculiar dynamical regime with an apparently chaotic behavior, which nevertheless allows for a deterministic description in the thermodynamic limit. In the present work, we tried to clarify the relation of the deterministic chaos in the finite size system and the spectral properties of the corresponding thermodynamic evolution equation. By a careful study of the Lyapunov spectra, we have demonstrated that chimera states are weakly hyperchaotic trajectories in the sense that their Lyapunov spectra contain a considerable number of positive Lyapunov exponents. When the system size grows, the hyperchaotic part of the spectrum tends to zero. We also have found that for $N \to \infty$ the whole Lyapunov spectrum has a well-defined limiting behavior, which can be associated with the spectral properties of the thermodynamic limit equation.
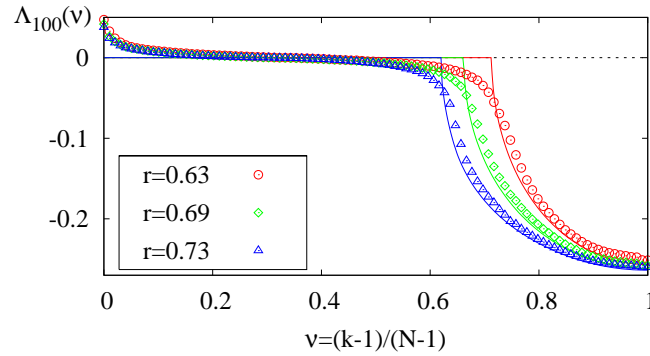
5 Acknowledgment

Figure 9: (Color) Comparison of the Lyapunov spectra (color dots) from Figure 2 with the corresponding Lyapunov spectrum functions $\Lambda_\infty(\nu)$ (color lines) defined by (20).

References

[1] A. Compte, N. Brunel, P. S. Goldman-Rakic, and X.-J. Wang, Cerebral Cortex **10**, 910 (2000).

[2] A. Renart, P. Song, and X.-J. Wang, Neuron **38**, 473 (2003).

[3] C. C. Chow and S. Coombes, SIAM J. Appl. Dynam. Syst. **5**, 552 (2006).

[4] H. Sakaguchi, Phys. Rev. E **73**, 031907 (2006).

[5] D. Barkley and L. S. Tuckerman, Phys. Rev. Lett. **94**, 014502 (2005).

[6] Y. Kuramoto and D. Battogtokh, Nonlinear Phenom. Complex Syst. **5**, 380 (2002).

[7] Y. Kuramoto, *Chemical Oscillations, Waves, and Turbulence* (Springer, Berlin Heidelberg New York, 1984).

[8] S. H. Strogatz, Physica D **143**, 1 (2000).

[9] J. A. Acerbrón, L. L. Bonilla, C. J. Pérez-Vicente, F. Ritort, and R. Spigler, Rev. Mod. Phys. **77**, 137 (2005).

[10] R. Mirollo and S. H. Strogatz, J. Nonlinear Sci. **17**, 309 (2007).

[11] Y. Kuramoto, in *Nonlinear Dynamics and Chaos: Where Do We Go from Here?*, edited by S. J. Hogan, A. R. Champneys, B. Krauskopf, M. di Bernardo, R. E. Wilson, H. M. Osinga, and M. E. Homer (Institute of Physics, Bristol, U.K., 2003), p. 209.

[12] S. I. Shima and Y. Kuramoto, Phys. Rev. E **69**, 036213 (2004).

[13] D. M. Abrams and S. H. Strogatz, Phys. Rev. Lett. **93**, 174102 (2004).

[14] D. M. Abrams and S. H. Strogatz, Int. J. Bif. and Chaos **16**, 21 (2006).

[15] Y. Kawamura, Phys. Rev. E **75**, 056204 (2007).

[16] D. M. Abrams, R. Mirollo, S. H. Strogatz, and D. A. Wiley, Phys. Rev. Lett. **101**, 084103 (2008a).

[17] D. M. Abrams, R. Mirollo, S. H. Strogatz, and D. A. Wiley, Phys. Rev. Lett. **101**, 129902 (2008b).

[18] G. C. Sethia, A. Sen, and F. M. Atay, Phys. Rev. Lett. **100**, 144102 (2008).

[19] C. R. Laing, Chaos **19**, 013113 (2009a).

[20] C. R. Laing, Physica D **238**, 1569 (2009b).

[21] C. R. Laing, Phys. Rev. E **81**, 066221 (2010).

[22] E. A. Martens, C. R. Laing, and S. H. Strogatz, Phys. Rev. Lett. **104**, 044101 (2010).

[23] E. A. Martens, Phys. Rev. E **82**, 016216 (2010).

[24] J. H. Sheeba, V. K. Chandrasekar, and M. Lakshmanan, Phys. Rev. E **79**, 055203 (2009).

[25] O. E. Omel'chenko, Y. L. Maistrenko, and P. A. Tass, Phys. Rev. Lett. **100**, 044105 (2008).

[26] O. E. Omel'chenko, Y. L. Maistrenko, and P. A. Tass, Phys. Rev. E **82**, 066201 (2010a).

[27] O. E. Omel'chenko, M. Wolfrum, and Y. L. Maistrenko, Phys. Rev. E **81**, 065201 (2010b).

[28] G. Bordyugov, A. Pikovsky, and M. Rosenblum, Phys. Rev. E **82**, 035205 (2010).

[29] A. E. Motter, Nature Physics **6**, 165 (2010).

[30] E. Ott, *Chaos in dynamical systems* (Cambridge University Press, Cambridge, 2002).

[31] F. Ginelli, P. Poggi, A. Turchi, H. Chaté, R. Livi, and A. Politi, Phys. Rev. Lett. **99**, 130601 (2007).

[32] P. Grassberger and I. Procaccia, Physica D **9**, 189 (1983).

[33] H. Fujisaka and T. Yamada, Prog. Theor. Phys. **69**, 32 (1983).

[34] V. Ahlers, R. Zillmer, and A. Pikovsky, Phys. Rev. E **63**, 036213 (2001).

[35] O. V. Popovych, Y. L. Maistrenko, and P. A. Tass, Phys. Rev. E **71**, 065201 (2005).

[36] S. Olmi, R. Livi, A. Politi, and A. Torcini, Phys. Rev. E **81**, 046119 (2010).

[37] R. Livi, A. Politi, and S. Ruffo, J. Phys. A: Math. Gen. **19**, 2033 (1986).

[38] P. Grassberger, Phys. Scr. **40**, 346 (1989).

[39] S. H. Strogatz and R. E. Mirollo, J. Statist. Phys. **63**, 613 (1991).

[40] F. Christiansen and H. H. Rugh, Nonlinearity **10**, 1063 (1997).

[41] A. Pikovsky and M. Rosenblum, Phys. Rev. Lett. **101**, 264103 (2008).

[42] S. Watanabe and S. H. Strogatz, Phys. Rev. Lett. **70**, 2391 (1993).

[43] S. Watanabe and S. H. Strogatz, Physica D **74**, 197 (1994).

[44] E. Ott and T. M. Antonsen, Chaos **18**, 037113 (2008).

[45] E. Ott and T. M. Antonsen, Chaos **19**, 023117 (2009).

[46] T. Kato, *Perturbation theory for linear operators* (Springer, Berlin Heidelberg New York, 1966).